Discover Applied Sciences

Research

Sustainable synthesis of silver nanoparticles using *Cynometra ramiflora* leaf extract for methyl orange degradation

Raja Selvaraj[1] · Stuthi A. Shetty[1] · Gokulakrishnan Murugesan[2] · Thivaharan Varadavenkatesan[3] · Ramesh Vinayagam[1]

Received: 28 March 2025 / Accepted: 5 June 2025
Published online: 18 June 2025
© The Author(s) 2025 OPEN

Abstract
This study presents an eco-friendly method to synthesize silver nanoparticles (AgNPs) utilizing the leaf extract of *Cynometra ramiflora* as a bio-reducing agent. A distinct 431 nm surface plasmon resonance signal confirmed the formation of AgNPs. SEM images portrayed uniformly distributed spherical nanoparticles with smooth surfaces. EDX analysis showed a prominent peak at 3 keV, confirming elemental silver. TEM analysis indicated that most AgNPs were 10–25 nm in size, with a mean size of 18.84 nm. XRD confirmed the face-centered cubic nature of the AgNPs. The d-spacing for the (111) plane was found to be 0.2287 nm, in agreement with standard reference values. FTIR analysis demonstrated signals at 3301, 1637, and 843 cm^{-1}, indicating the engagement of functional moieties in reducing and capping the AgNPs. The synthesized AgNPs had a high zeta potential (− 18.2 mV), revealing good stability. The AgNPs demonstrated excellent catalytic potential in the presence of $NaBH_4$, degrading approximately 95% of methyl orange dye within 15 min, following a pseudo-first-order kinetic model with a kinetic constant of 0.186 min^{-1}.

Keywords Silver nanoparticles · *Cynometra ramiflora* · Green synthesis · Catalytic degradation · Methyl Orange · Wastewater treatment

1 Introduction

Nanotechnology, a rapidly advancing field in recent years, focuses on materials at the nanoscale (100 nm or smaller). These tiny particles possess a significantly high surface area relative to their volume, leading to enhanced properties like catalytic activity, and chemical stability [1]. Metallic nanoparticles display various physical and chemical properties that make them valuable for researchers across many disciplines, involving biosensors, electronics, healthcare, textiles, food science, environmental science, and agriculture [2]. Among various precious metals, silver is often the preferred choice for nanoparticle applications due to its distinct properties, including its strong catalytic ability, cost-effectiveness, high chemical stability, and good conductivity [3].

Silver nanoparticles (AgNPs) as catalysts are widely used for the environmental remediation of various toxic dyes. Methyl Orange (MO), a hazardous azo dye soluble in water, is challenging to eliminate from aquatic environments using conventional techniques because it is stable and does not readily break down. Exposure to MO can cause adverse health

✉ Thivaharan Varadavenkatesan, thivaharan.v@manipal.edu; ✉ Ramesh Vinayagam, ramesh.v@manipal.edu | [1]Department of Chemical Engineering, Manipal Institute of Technology, Manipal Academy of Higher Education, Manipal, Karnataka 576104, India. [2]Department of Biotechnology, M.S. Ramaiah Institute of Technology, Bengaluru, Karnataka 560054, India. [3]Department of Biotechnology, Manipal Institute of Technology, Manipal Academy of Higher Education, Manipal, Karnataka 576104, India.

effects, and high concentrations can be fatal [4]. Various physical and chemical methods have been devised to treat industrial dye effluents. However, the majority of these methods are hampered by problems like secondary pollution, intricate procedures, substantial expenses, low efficiency in dye removal, and the generation of large volumes of toxic sludge and intermediate compounds, making them less viable for practical use [5]. To address the challenges of effectively removing dyes from wastewater, a new and efficient technique has emerged: the reduction of dyes into harmless compounds using $NaBH_4$, catalyzed by AgNPs, offering improvements over existing treatment methods [6]. $NaBH_4$ is commonly employed in laboratory-scale dye degradation studies due to its strong reducing capabilities, and when used in controlled conditions, it poses minimal environmental risk. Its decomposition products are relatively benign under standard conditions, especially when handled properly in buffered or aqueous environments.

The synthesis of AgNPs generally employs two prime strategies: the top-down and bottom-up approaches [7]. These encompass different methodologies including physical, chemical, and biological methods. Among these, the biological or green synthesis approach utilizes both microbes and plants and has gained significant attention over conventional physical and chemical methods. This preference is driven by its key advantages, including enhanced safety, environmentally friendly protocols that produce non-hazardous by-products, and the requirement for mild reaction conditions [8]. However, plant-based synthesis is increasingly favored due to its non-toxic nature, eco-friendly characteristics, and cost-effectiveness [9]. While microorganisms can be used, their need for sterile culture conditions makes them less desirable compared to plants.

Plants serve as effective reducing agents in AgNPs preparation owing to the presence of a diverse range of biomolecules (e.g., proteins, flavonoids, polyphenols, and other phytochemicals) that readily donate electrons [10]. A significant amount of recent scientific work focuses on the preparation of AgNPs utilizing plant-derived extracts, as evidenced by studies reporting the use of plants like *Rubus discolor* [11], *Operculina turpethum* [12], *Mitragyna parvifolia* [13], *Olea europaea* [14], *Drymaria cordata* [15], and *Boerhavia diffusa* [16], among others, for this eco-friendly approach. *Cynometra ramiflora* is traditionally significant in treating conditions like diabetes and hypertension, with different parts of the plant used for distinct medicinal purposes. Recent bioassays have revealed its antinociceptive, antibacterial, antioxidant, cytotoxic, and antihyperglycemic properties [17]. *C. ramiflora* possesses a rich profile of natural bioactive components, including alkaloids, flavonoids, sterols, terpenoids, and phenolic compounds [17, 18]. These biomolecules make it a promising candidate for green nanoparticle synthesis, yet its potential remains largely unexplored. To the best of our knowledge, this is the first report on the green synthesis of silver nanoparticles using *C. ramiflora* leaf extract and their application for the catalytic degradation of MO dye. This study not only introduces a novel plant system for nanoparticle fabrication but also demonstrates its high catalytic efficiency, offering a sustainable and cost-effective alternative for wastewater treatment applications. This research has two primary objectives: first, the preparation and comprehensive characterization of AgNPs using the reducing capabilities of *C. ramiflora* leaf extract; second, the exploration of the catalytic ability of these AgNPs to degrade MO dye.

2 Materials and methodology

2.1 Materials

C. ramiflora leaves served as the raw material for AgNPs preparation. Fresh leaves were taken from the institute surroundings. Analytical reagent grade chemicals, including Methyl Orange dye (HiMedia), $AgNO_3$ (Merck), and $NaBH_4$ (SRL), were used without any further purifications. All the reagents were made using distilled water.

2.2 *Cynometra ramiflora* Leaf Extract (CRLE) preparation

Cynometra ramiflora Leaf Extract (CRLE) was prepared according to our earlier study with few modifications [19]. Briefly, the leaves were initially cleaned thoroughly with tap water with subsequent multiple rinses with distilled water to eliminate any residual contaminants. After being cut into small pieces, 20 g of the cleaned leaves were heated with 200 mL of water in a water bath at 80 °C for 30 min. The contents were subsequently filtered with Whatman No. 1 filter paper to separate the residual leaves, and the resulting filtrate was refrigerated for subsequent use.

2.3 Synthesis of *C. ramiflora*-derived silver nanoparticles (CR-AgNPs)

For the synthesis of *C. ramiflora*-derived silver nanoparticles (CR-AgNPs), a slightly modified procedure given in the literature was followed [19], wherein, 5 mL of CRLE was combined with 45 mL of a 1 mM $AgNO_3$ solution. The contents were subjected to a controlled heating of 80 °C for 30 min in a water bath without any pH adjustment. The formation of AgNPs was confirmed visually by monitoring the color changes. The resulting solution was designated as CR-AgNPs.

2.4 Characterization of CR-AgNPs

The CR-AgNPs that were synthesized underwent various characterization techniques to verify their formation and assess their properties. UV–vis spectra were recorded using a Shimadzu UV-1900 spectrometer to identify the surface plasmon resonance (SPR) peak. Morphological analysis and size distribution were examined using a JEM-2100 plus TEM (JEOL, Japan). Surface morphology was examined with an EVO MA18 instrument. Elemental compositions were analyzed using an Oxford Instruments system attached to the SEM (EDX). The crystalline structure was analyzed with a Rigaku Miniflex 600 X-ray diffractometer. Finally, FTIR spectra were recorded using a Shimadzu-8400S spectrophotometer to examine the functional moieties in the CRLE and on the surface of the CR-AgNPs. The stability and charge properties were determined using Dynamic Light Scattering technique (DLS, Malvern Zetasizer Nano).

2.5 Catalytic reduction of MO dye

The catalytic potential of the CR-AgNPs was examined by monitoring the degradation of MO dye in the presence of $NaBH_4$ [19]. The degradation reactions were performed in a standard cuvette containing 3 mL of a 25 mg/L MO dye. Each reaction was commenced by introducing 0.05 mL of the CR-AgNPs and 0.1 mL of a freshly prepared 100 mM $NaBH_4$ solution. For the control experiment, the reaction was carried out with the same components except CR-AgNPs. To calculate the percentage degradation of MO dye at each time point, Eq. 1 was used. This equation typically relates the initial concentration of the dye (C_0) to its concentration at a given time (C_f), allowing for the determination of the degradation efficiency.

$$\% \text{ Degradation} = \frac{C_{0-}C_f}{C_0} \times 100 \tag{1}$$

To determine the rate constant (k), a pseudo-first-order kinetic equation was employed (Eq. 2).

$$ln\frac{C_0}{C_f} = -kt \tag{2}$$

By plotting ln (C_0/C_f) versus t, the value of k was calculated from the slope.

3 Results and discussions

3.1 UV–vis spectroscopic results

The UV–vis spectral analysis of CR-AgNPs, with deionized water as a control, is presented in Fig. 1. As the reaction progressed, the mixture of $AgNO_3$ solution and leaf extract transitioned from yellow to dark brown which confirmed the successful formation of AgNPs, indicating the Ag^+ reduction to Ag^0 by the CRLE. A distinct SPR signal at 431 nm indicates the formation of AgNPs, attributed to the surface electron oscillations in nanoparticles when they interact with light. Silver nanoparticles are characterized by their ability to provide an SPR absorbance signal within the 400 to 450 nm spectral range [20]. The obtained SPR value aligns with literature, such as AgNPs synthesized using *Persea americana* seed extract (430 nm) [21], and *Eucalyptus globulus* leaf extract (431 nm) [22]. The broadened SPR peak suggests a polydisperse size distribution of the synthesized CR-AgNPs. The observed decrease in peak values at 267 and 353 nm points to the critical

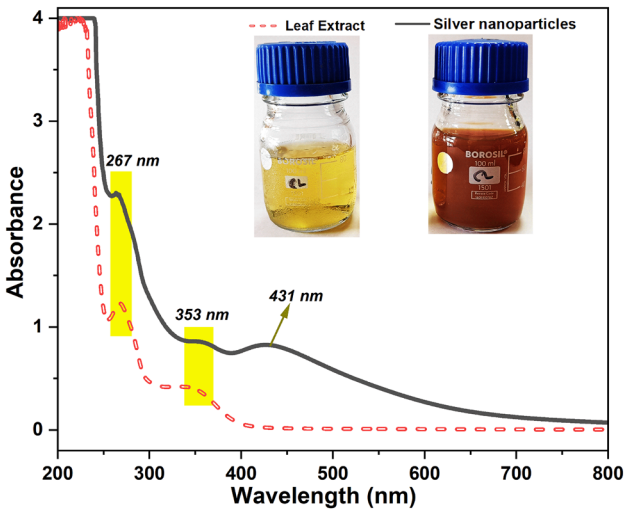


Fig. 1 UV–vis absorption spectra of CRLE and CR-AgNPs

involvement of biomolecules, such as polyphenols and flavonoids, in the dual process of reducing silver ions to AgNPs and subsequently stabilizing them against aggregation.

3.2 SEM and EDX analyses

Figure 2a displays a representative SEM image of CR-AgNPs, showcasing a uniform distribution of spherical nanoparticles with smooth surfaces across the observed area. The particles appear as bright, distinct entities against a darker background, indicating high contrast and suggesting a specific material composition. The size distribution of the CR-AgNPs is relatively homogeneous, and the image visualizes their size within the nanometer range, confirming successful synthesis. Additionally, the absence of significant agglomeration or large aggregates indicates effective control over the synthesis process, resulting in well-dispersed nanoparticles. Similar structural and morphological features have been observed for AgNPs synthesized from extracts of *Hebeloma excedens* mushroom [23], *Garcinia mangostana* [24], and *Moringa oleifera* [25].

Figure 2b presents the EDX image of CR-AgNPs, showing a prominent signal at 3 keV, which corresponds to the characteristic signal for silver [26]. This strong signal confirms that silver is the primary component of the synthesized nanoparticles, supporting SEM observations. Additionally, minor peaks are observed around 0.3 keV (attributed to carbon), 0.5 keV (attributed to oxygen), and 2.6 keV (attributed to chlorine). These elements likely originate from biomolecules of the CRLE that are attached to the surface of the CR-AgNPs [23, 25], suggesting they may be capping the nanoparticles.

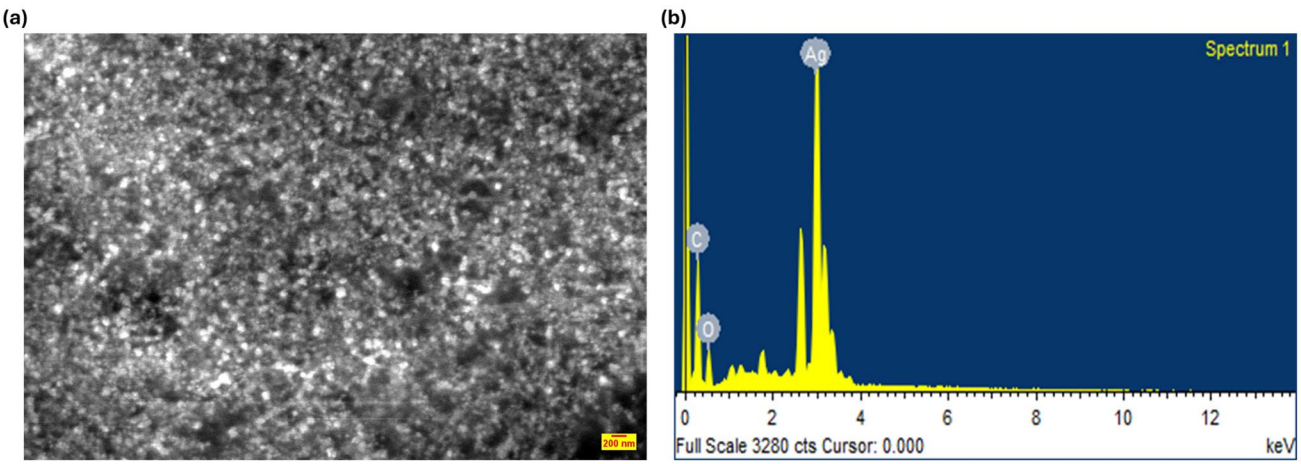


Fig. 2 **a** SEM image and **b** EDX analysis of CR-AgNPs

3.3 TEM analysis of CR-AgNPs

TEM image (Fig. 3a) shows mostly spherical, well-dispersed nanoparticles with minimal aggregation. This observation suggests that the biomolecules of CRLE are effective in capping and stabilizing the nanoparticles, thereby preventing agglomeration. Similar to the current study, *Bauhinia variegata* leaf extract-mediated AgNPs displayed a homogenous, spherical, and polycrystalline morphology [27]. To gain a more precise understanding of the size distribution, the TEM image was analyzed to generate a histogram (Fig. 3b). This analysis confirms that the majority of the CR-AgNPs fall within the 10–25 nm range, with a mean particle size of 18.84 ± 8.67 nm, which is comparable to previous reports such as silver nanoparticles synthesized using *Rubia cordifolia* L. leaf extract, which exhibited an average size of 20.98 nm [28].

This narrow size distribution further indicates a controlled synthesis process. Figure 3c depicts the Selected Area Electron Diffraction (SAED) patterns, which display clear concentric rings, a characteristic feature of crystalline materials. These rings correspond to different lattice planes of the crystal structure of the CR-AgNPs, indicating their polycrystalline nature [29]. The fast Fourier transform (FFT) analysis of the CR-AgNPs is presented in the higher magnification TEM image shown in Fig. 3d. The observation of well-defined and consistent lattice fringes provides evidence of the high degree of crystallinity in the silver nanoparticles. By measuring the interplanar distance between the lattice planes, a d-spacing of 0.241 nm was determined, which aligns with the singular reciprocal points observed in the FFT pattern. This measured value of 0.241 nm supports the identification of the material as face-centered cubic (fcc) silver, given that it aligns closely with the expected (111) lattice spacing of 0.2359 nm [30].

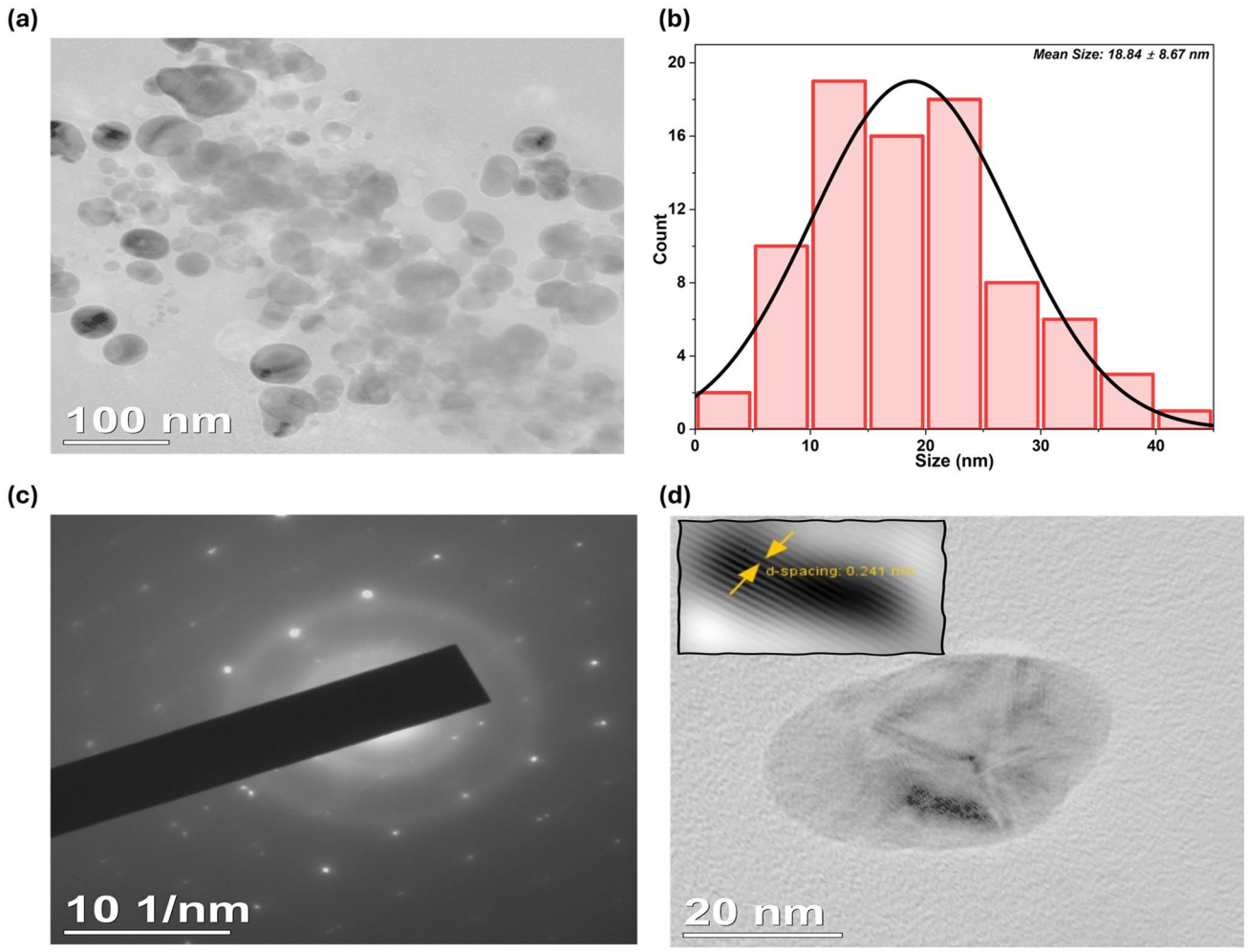


Fig. 3 **a** TEM image **b** size distribution **c** SAED Pattern and **d** Higher magnification and the corresponding FFT pattern of the CR-AgNPs

3.4 XRD analysis of CR-AgNPs

XRD analysis (Fig. 4) of the CR-AgNPs reveals the characteristic peaks associated with the fcc structure of silver. The presence of prominent signals at 2θ angles of 39.32°, 45.52°, 65.51°, and 78.46° confirms the presence of fcc silver, as these peaks correspond to the respective crystallographic planes of (111), (200), (220), and (311). The observed signals strongly confirm the crystalline nature of the synthesized AgNPs and show a good match with the standard reference data provided in JCPDS card number 04-0783 [31]. The strong correlation between the XRD results and the SAED pattern provides compelling evidence that the CR-AgNPs are polycrystalline. In addition to the silver peaks, the presence of peaks at 47.56°, 56.04°, and 58.68° may correspond to crystalline phases of residual phytochemicals or bioorganic compounds derived from the leaf extract of *C. ramiflora*. These peaks could originate from the partial crystallization of plant-derived compounds such as flavonoids, terpenoids, or phenolic compounds on the surface of the AgNPs. Their presence does not interfere with the main silver peaks, suggesting that the metallic core remains pure and crystalline. However, the presence of these signals may indicate surface functionalization, which could enhance the stability, dispersibility, or even the catalytic performance of the AgNPs by preventing aggregation and introducing active surface sites. This interpretation is supported by previous reports on green-synthesized nanoparticles, where plant extract residues contributed to secondary diffraction peaks [32, 33].

The average crystallite diameter of the CR-AgNPs, estimated with the Scherrer equation, was determined to be 19.51 nm, indicating that the synthesized nanoparticles are in the nanometer range. This closely matches the average particle size observed in TEM (18.84 nm). The size range observed for the CR-AgNPs is consistent with previous reports on silver nanoparticles produced using plant extracts. For example, AgNPs from *Santalum album* fruit extract had a mean crystallite diameter of 20 nm [34]. Likewise, AgNPs produced with leaf extract of *Artocarpus heterophyllus* exhibited a mean crystallite size of 20 nm [35]. The d-spacing for the (111) plane is calculated as 0.2287 nm, that is consistent with the d-spacing of 0.241 nm (FFT pattern) and the standard value for fcc silver. The lattice parameter determined was 0.39607 nm, which matches the standard value of 0.4086 nm for silver nanoparticles. The close match in lattice parameters further validates the successful formation of crystalline nanoparticles.

3.5 FTIR results

Figure 5 depicts the FTIR spectral images of the leaf extract and the CR-AgNPs, highlighting the functional moieties accountable to reduce and cap CR-AgNPs. The CRLE displays a signal at 3301 cm^{-1} for O–H stretching from phenolics [36], 1637 cm^{-1} for amide I bands arising due to carbonyl stretch in proteins [37], and 843 cm^{-1} for C–H bending in aromatics [38], indicating their involvement in Ag^{+} reduction and nanoparticle capping. In the AgNPs spectrum, the corresponding shifts to 3312, 1644, and 848 cm^{-1} indicate that the binding to the nanoparticle surface has changed the vibrational energies of the molecules, underscoring the importance of these groups in preventing nanoparticle aggregation. These spectral shifts suggest the involvement of hydroxyl, amide, and aromatic functional groups—likely

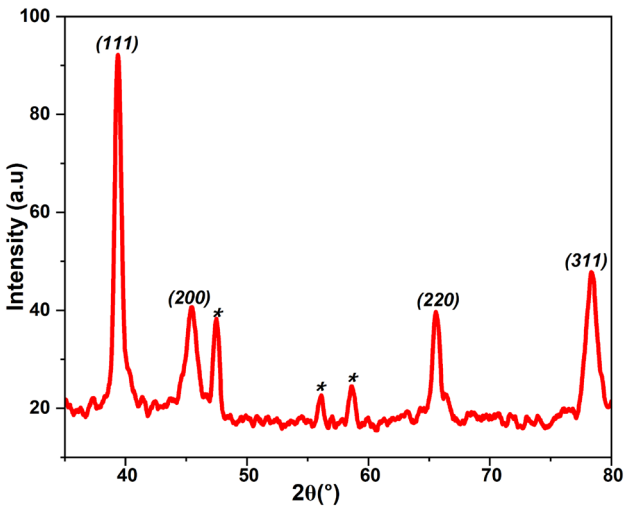


Fig. 4 XRD Pattern of CR-AgNPs

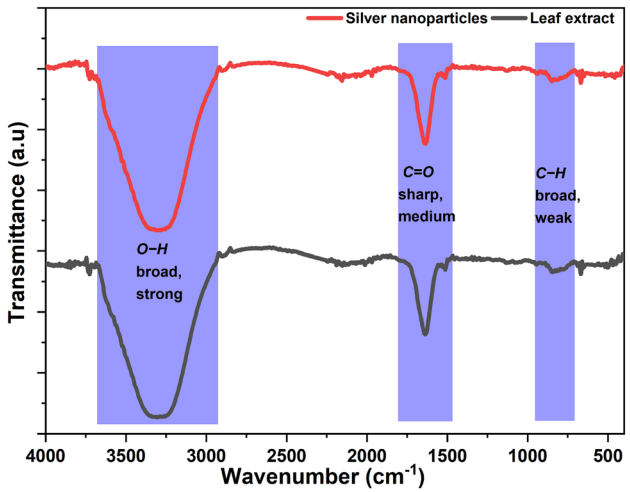


Fig. 5 FTIR Spectra of CRLE and CR-AgNPs

derived from phytochemicals such as flavonoids, terpenoids, and phenolic acids present in *C. ramiflora* extract—in the bioreduction of silver ions and capping of AgNPs. Flavonoids and polyphenols are known for their strong reducing capabilities due to hydroxyl groups, while terpenoids can assist in stabilizing nanoparticles via hydrophobic interactions and molecular capping. Therefore, the FTIR data not only confirms the participation of these functional groups but also point toward the active role of specific classes of bioactive compounds in the green synthesis and stabilization of CR-AgNPs.

3.6 Zeta potential analysis of CR-AgNPs

The stability of nanomaterials within an aqueous environment is critically dependent on the zeta potential value, an important indicator of surface charge. A high absolute zeta potential value implies a strong surface charge on nanoparticles, resulting in significant electrostatic repulsion. This repulsion prevents particle agglomeration, ensuring excellent colloidal dispersity and long-term stability [39]. Generally, zeta potential values more negative than – 30 mV or more positive than + 30 mV are considered highly stable, while values in the range of ± 15–30 mV suggest moderate stability due to sufficient electrostatic repulsion. The zeta potential value of the CR-AgNPs is depicted in Fig. 6. The CR-AgNPs exhibited a zeta potential of – 18.2 mV which falls within this moderate stability range, indicating that the particles possess adequate surface charge to resist aggregation under ambient conditions. Similarly, green synthesized AgNPs from different sources reported comparable values. For example, – 19.7 mV for green tea extract [40], – 19.1 mV for *Sambucus ebulus* extract [41], and – 12 mV for *Azadirachta indica* leaf extract [42]. Therefore, the observed moderately negative zeta potential confirms that the CR-AgNPs are electrostatically stabilized and likely to remain well-dispersed in suspension over time.

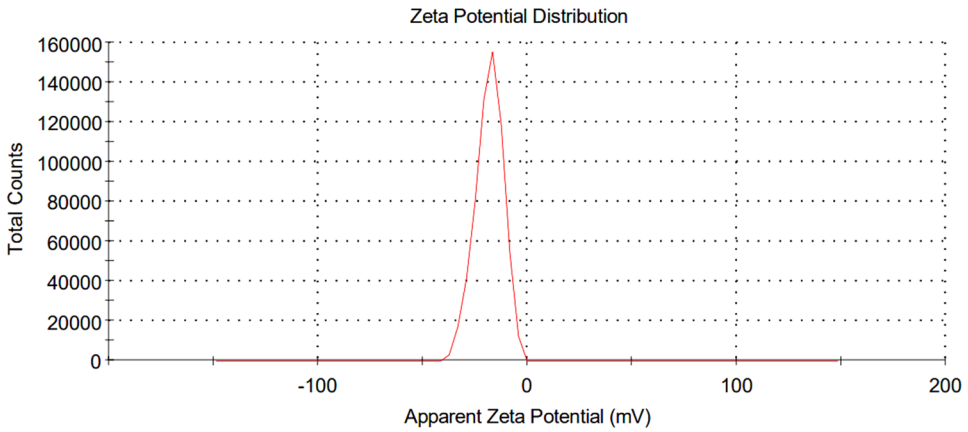


Fig. 6 Zeta Potential of CR-AgNPs

3.7 Catalytic degradation of MO dye

The CR-AgNPs-catalyzed degradation of MO by $NaBH_4$ was monitored using UV–vis spectra. Figure 7a illustrates the UV–vis spectra of the MO dye following the addition of $NaBH_4$, highlighting the reaction when the CR-AgNPs catalyst is not present. A characteristic absorption peak of MO is observed at 464 nm in the spectrum, corresponding to the azo bond (n → π* transition) [43]. No substantial reduction in the absorbance at 464 nm was seen over the 30 min, indicating a very slow reaction. The inset image in Fig. 7a, visually confirms the no color change in the dye solution after 30 min. Quantitative analysis (Fig. 7c) revealed a negligible MO removal of approximately 0.3% after 30 min. This indicates that $NaBH_4$ alone is not an effective reducing agent for MO under these experimental conditions, consistent with literature reports highlighting the kinetic barrier for this reaction [44].

The catalytic effect of CR-AgNPs on the reduction of MO by $NaBH_4$ is evident in Fig. 7b. Upon the addition of CR-AgNPs, a rapid decrease in the absorbance peak at 464 nm was witnessed over time. Within the first 15 min, the absorbance at 464 nm significantly diminished, indicating substantial degradation of the MO dye. Quantitative analysis (Fig. 7c) shows that approximately 95% of the MO dye was removed within 15 min. This significant enhancement in the reduction rate demonstrates the catalytic activity of the CR-AgNPs. The inset images in Fig. 7b, visually confirm this, showing a rapid

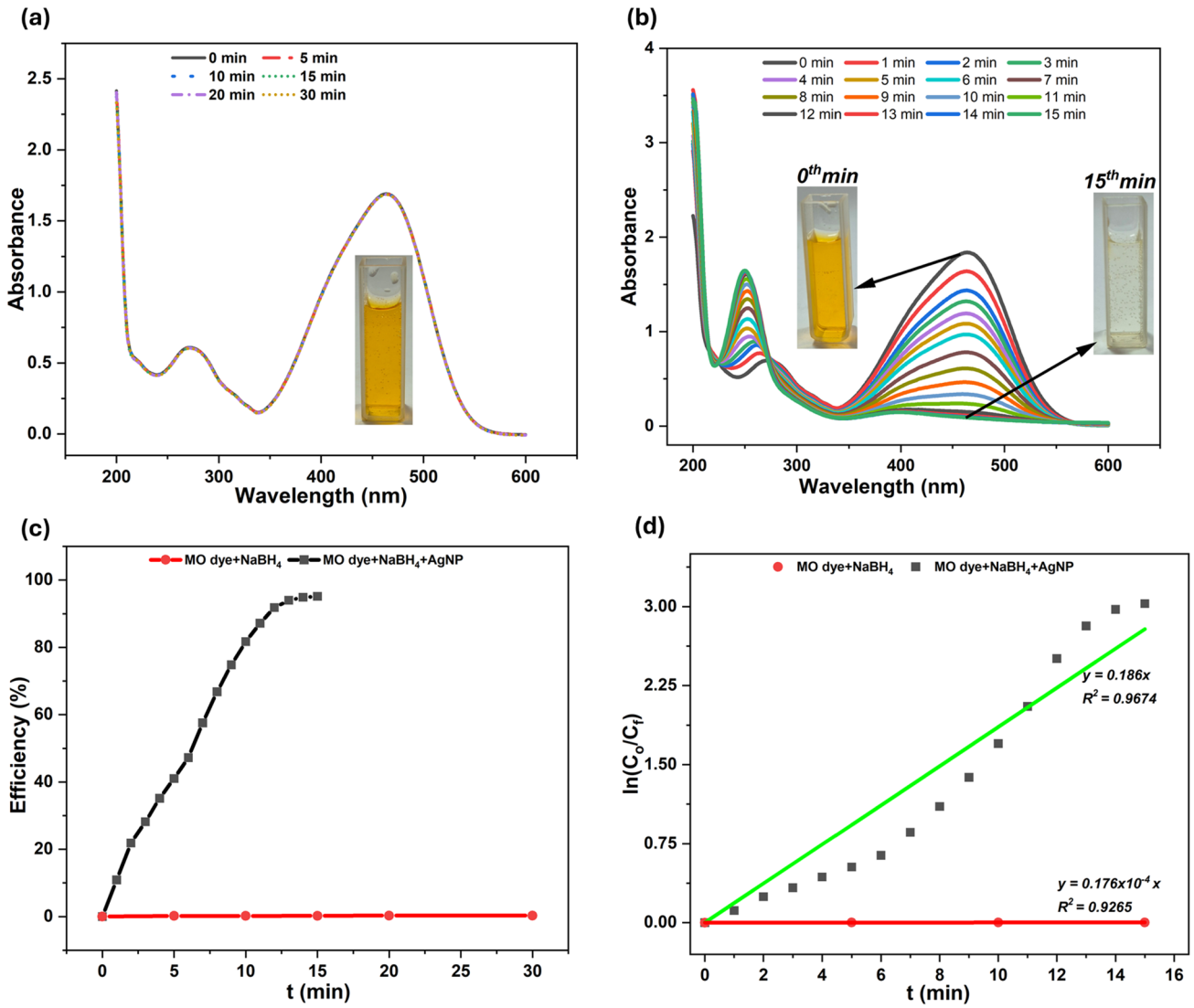


Fig. 7 Comparative analysis of MO dye degradation with and without CR-AgNPs: **a** and **b** spectral changes, **c** degradation efficiency, **d** Pseudo-first-order kinetic plot

decolorization of the solution from its native color to colorless within 15 min. Furthermore, careful observation of the spectra in Fig. 7b reveals a potential increase in absorbance in the region between 250 and 270 nm as the reaction progresses. This observation suggests the formation of degradation products. Specifically, the reduction of the azo (–N=N–) moiety within the MO dye likely involved the formation of a hydrazo intermediate (–NH–NH–), which subsequently underwent bond scission to produce colorless degradation products [45]. These colorless degradation products are known to absorb UV light in this shorter wavelength region.

The kinetics of the reaction were also investigated (Fig. 7d). The plot of $\ln(C_0/C_f)$ versus time for the AgNP-catalyzed reaction exhibits a linear relationship, suggesting a pseudo-first-order reaction for the MO dye concentration. The calculated rate constant (k) from the slope of this linear fit is 0.186 min^{-1} with a good correlation coefficient ($R^2 = 0.9674$). In contrast, the control reaction shows negligible change in $\ln(C_0/C_f)$ over time, consistent with its very slow reaction rate. To contextualize our findings, we compared our degradation kinetics with values reported in literature for AgNPs synthesized using different plant extracts. Studies have demonstrated the pseudo-first-order degradation of MO dye with AgNPs synthesized from various plant extracts. The degradation efficiency, as reflected in the rate constant, varies significantly depending on the plant source. For instance, Neethu et al. (2019) reported complete degradation of MO dye within 10 min using AgNPs derived from *Derris trifoliata* seed extract, corresponding to a high reaction rate [44]. Similarly, Rajasekar et al. (2022) achieved near-complete degradation in 11 min with AgNPs from *Heterotheca subaxillaris* flowers, reporting a rate constant of 0.120 min^{-1} [46]. In contrast, Sherin et al. (2020) observed slower degradation—taking 60 min—with AgNPs synthesized from *Terminalia bellerica* kernel extract, and a rate constant of just 0.0286 min^{-1} [47]. These comparisons highlight the superior performance of our CR-AgNPs, which exhibit a higher degradation rate ($k = 0.186\ min^{-1}$) than many previously reported green-synthesized AgNP systems. The data underscores the significant role of plant extract composition in influencing the catalytic efficiency of AgNPs.

The degradation process occurs through an electron relay mechanism, with CR-AgNPs serving as effective electron mediators [48]. In this mechanism, $NaBH_4$ acts as the electron donor, while MO dye functions as the electron acceptor. Direct electron transfer from $NaBH_4^-$ to MO dye is kinetically hindered. However, the surface of CR-AgNPs facilitates this transfer by accepting electrons from BH_4^- and subsequently transferring them to MO dye molecules. This action reduces the azo bond (–N=N–) in the dye molecule, leading to its degradation into colorless amines.

4 Conclusion

The present study successfully demonstrated a facile and eco-friendly synthesis of AgNPs using *Cynometra ramiflora* leaf extract. The synthesized AgNPs were characterized using multiple techniques to confirm their morphology, structure, stability, and catalytic efficiency. UV–Vis spectroscopy revealed a SPR peak at 431 nm, indicating the successful formation of AgNPs. TEM analysis confirmed well-dispersed, spherical nanoparticles with a mean size of 18.84 nm, while XRD analysis revealed a face-centered cubic structure with a crystallite size of 19.51 nm, closely matching TEM observations. FTIR spectra highlighted the involvement of functional moieties such as hydroxyl and amide groups in the bioreduction and capping of AgNPs. The nanoparticles exhibited moderate colloidal stability as indicated by a zeta potential of – 18.2 mV. Notably, the prepared AgNPs displayed excellent catalytic performance to degrade MO dye, achieving approximately 95% reduction in 15 min and following pseudo-first-order kinetics. The results of this research demonstrate the potential of utilizing *C. ramiflora* leaf extract as an efficient and sustainable method for producing highly stable and catalytically active silver nanoparticles, offering a promising avenue for environmental applications. Furthermore, the simplicity and green nature of this synthesis method suggest potential scalability; however, challenges such as maintaining batch-to-batch consistency, optimizing reaction conditions, and ensuring eco-safety at industrial levels must be addressed in future studies to facilitate commercial implementation.

Author contribution R.S performed the experiments and wrote the main manuscript. S.A.S performed the experiments. G.M analyzed the data and wrote the revised version of the manuscript. T.V. analyzed the data and wrote the revised version of the manuscript. R.V. supervised the project and wrote the revised version of the manuscript.

Funding Open access funding provided by Manipal Academy of Higher Education, Manipal. None.

Data availability The authors confirm that the entire dataset supporting the conclusions of this research is contained in the manuscript itself.

Declarations

Ethics approval and consent to Participate Not applicable.

Consent for publication Not applicable.

Competing interests The authors declare no competing financial interest.

Clinical trial Not applicable.

Plant Guideline The authors affirm that the utilization of plants or plant parts in this research adheres to all applicable international, national, and institutional regulations.

Permission for collecting plants/plant parts The leaves of the tree were taxonomically identified and authenticated by Dr. Gayathri Pai,Department of Botany, MGM College, Udupi, India. Given that the tree is widely recognized, common,and not under any protection, there was no need for collection permits or licenses. Furthermore, due to its well-known status, no vouchers were deposited in a herbarium.

Plant source Details regarding all plant names and their sources are provided in the Methodology section of this document.

Declaration of generative AI and AI-assisted tools in writing The authors utilized ChatGPT for grammar checking and sentence refinement for the preparation of this article. Following the usage of the tool, the contents were carefully reviewed and modified. They assume complete accountability for the final contents of this manuscript.

Open Access This article is licensed under a Creative Commons Attribution 4.0 International License, which permits use, sharing, adaptation, distribution and reproduction in any medium or format, as long as you give appropriate credit to the original author(s) and the source, provide a link to the Creative Commons licence, and indicate if changes were made. The images or other third party material in this article are included in the article's Creative Commons licence, unless indicated otherwise in a credit line to the material. If material is not included in the article's Creative Commons licence and your intended use is not permitted by statutory regulation or exceeds the permitted use, you will need to obtain permission directly from the copyright holder. To view a copy of this licence, visit http://creativecommons.org/licenses/by/4.0/.

References

1. Mehra V, Kumar S, Tamang AM, Chandraker SK. Green synthesis of gold nanoparticles (AuNPs) by using plant extract and their biological application: a review. Bionanoscience. 2024;15:18. https://doi.org/10.1007/s12668-024-01703-7.
2. Gola D, Kriti A, Bhatt N, Bajpai M, Singh A, Arya A, Chauhan N, Srivastava SK, Tyagi PK, Agrawal Y. Silver nanoparticles for enhanced dye degradation. Curr Res Green Sustain Chem. 2021;4:100132. https://doi.org/10.1016/j.crgsc.2021.100132.
3. Chandraker SK, Ghosh MK, Lal M, Shukla R. A review on plant-mediated synthesis of silver nanoparticles, their characterization and applications. Nano Express. 2021;2:22008. https://doi.org/10.1088/2632-959X/ac0355.
4. Shah RK. Efficient photocatalytic degradation of methyl orange dye using facilely synthesized α-Fe_2O_3 nanoparticles. Arab J Chem. 2023;16:104444. https://doi.org/10.1016/j.arabjc.2022.104444.
5. Jara YS, Mekiso TT, Washe AP. Highly efficient catalytic degradation of organic dyes using iron nanoparticles synthesized with *Vernonia amygdalina* leaf extract. Sci Rep. 2024;14:6997. https://doi.org/10.1038/s41598-024-57554-5.
6. Konduri VV, Kalagatur NK, Gunti L, Mangamuri UK, Kalagadda VR, Poda S, Krishna SBN. Green synthesis of silver nanoparticles from *Hibiscus tiliaceus* L. Leaves and their applications in dye degradation, antioxidant, antimicrobial, and anticancer activities. S Afr J Bot. 2024;168:476–87. https://doi.org/10.1016/j.sajb.2024.03.035.
7. Kaur N, Kumar R, Alhan S, Sharma H, Singh N, Yogi R, Chhokar V, Beniwal V, Kumar Ghosh M, Kumar Chandraker S, Rustagi S, Kumar A. *Lycium shawii* mediated green synthesis of silver nanoparticles, characterization and assessments of their phytochemical, antioxidant, antimicrobial properties. Inorg Chem Commun. 2024;159:111735. https://doi.org/10.1016/j.inoche.2023.111735.
8. Githala CK, Raj S, Dhaka A, Mali SC, Trivedi R. Phyto-fabrication of silver nanoparticles and their catalytic dye degradation and antifungal efficacy. Front Chem. 2022;10: 994721.
9. Kumar Chandraker S, Lal M, Kumar Ghosh M, Ram T, Paliwal R, Shukla R. Biofabrication of spherical silver nanoparticles using leaf extract of *Plectranthus barbatus* Andrews: characterization, free radical scavenging, and optical properties. Inorg Chem Commun. 2022;142:109669. https://doi.org/10.1016/j.inoche.2022.109669.
10. Bharathi D, Lee J, Karthiga P, Mythili R, Devanesan S, AlSalhi MS. Kiwi fruit peel biowaste mediated green synthesis of silver nanoparticles for enhanced dye degradation and antibacterial activity. Waste Biomass Valorization. 2024;15:1859–68. https://doi.org/10.1007/s12649-023-02328-9.
11. Ghasemi S, Dabirian S, Kariminejad F, Koohi DE, Nemattalab M, Majidimoghadam S, Zamani E, Yousefbeyk F. Process optimization for green synthesis of silver nanoparticles using Rubus discolor leaves extract and its biological activities against multi-drug resistant bacteria and cancer cells. Sci Rep. 2024;14:4130. https://doi.org/10.1038/s41598-024-54702-9.

12. Bawazeer S. Green synthesis: an eco-friendly approach for the synthesis of silver nanoparticles functionalized with *Operculina turpethum* and it's in vitro and in vivo biological activities. Int J Nanomed. 2025;20:2991–3005. https://doi.org/10.2147/IJN.S507134.
13. Dwivedi A, Sinchan D, Vaishali T, Varsha Y, Sunil J, Vivekananda M, Souvik M, Swaha S, Debadatta M, Alakh S, Mantra Prasad S, Sanjay-Kumar M, Sneha S, Manoj G, Mohsin K, MuhammadDelwar H, Patra A. Microwave-assisted green synthesis of silver nanoparticles using *Mitragyna parvifolia* bark extract and their biological activities: an economical and environment-friendly approach. Green Chem Lett Rev. 2024;17:2395919. https://doi.org/10.1080/17518253.2024.2395919.
14. Hashmi SS, Ibrahim M, Adnan M, Ullah A, Khan MN, Kamal A, Iqbal M, Kaplan A, Assad N, Elshikh MS, Almutairi SM, Zaman W. Green synthesis of silver nanoparticles from *Olea europaea* L. extracted polysaccharides, characterization, and its assessment as an antimicrobial agent against multiple pathogenic microbes. Open Chem. 2024. https://doi.org/10.1515/chem-2024-0016.
15. Arya A, Chahar D, Bhakuni K, Vandana S, Kumar S, Venkatesu P. Green synthesis of silver nanoparticles using *Drymaria cordata* and their biocompatibility with hemoglobin: a therapeutic potential approach. ACS Appl Bio Mater. 2024;7:977–89. https://doi.org/10.1021/acsabm.3c00974.
16. James JM, Yagoo A, Vilvest J, Jessie AAA. Green synthesis of silver nanoparticles using *Boerhavia diffusa* plant and the potential of its antioxidant and anticancer efficacy. Pharmacol Res Nat Prod. 2025;6:100142. https://doi.org/10.1016/j.prenap.2025.100142.
17. Abdus Samadd M, Rifaet Hossain M, Abdullah Taher M, Mahmudul Hasan M, Haque S, Islam Rafid M, Solaiman Hossain M, AshrafulIslam M, Khan M. Multifaceted chemico-pharmacological insights into *Cynometra ramiflora* L: unveiling its GC-MS, cytotoxic, thrombolytic, anti-inflammatory, antioxidant, anti-diarrheal, hypoglycemic, and analgesic potentials. Nat Prod Commun. 2024;19:19345. https://doi.org/10.1177/1934578X241257377.
18. Sabiha S, Serrano R, Hasan K, Moreira da Silva IB, Rocha J, Islam N, Silva O. The genus cynometra: a review of ethnomedicine, chemical, and biological data. Plants. 2022. https://doi.org/10.3390/plants11243504.
19. Varadavenkatesan T, Nagendran V, Vinayagam R, Goveas LC, Selvaraj R. Effective degradation of dyes using silver nanoparticles synthesized from *Thunbergia grandiflora* leaf extract. Bioresour Technol Rep. 2024;27:101914. https://doi.org/10.1016/j.biteb.2024.101914.
20. Sukweenadhi J, Setiawan KI, Avanti C, Kartini K, Rupa EJ, Yang D-C. Scale-up of green synthesis and characterization of silver nanoparticles using ethanol extract of *Plantago major* L. leaf and its antibacterial potential, South African. J Chem Eng. 2021;38:1–8. https://doi.org/10.1016/j.sajce.2021.06.008.
21. Rajkumar G, Sundar R. Biogenic one-step synthesis of silver nanoparticles (AgNPs) using an aqueous extract of *Persea americana* seed: characterization, phytochemical screening, antibacterial, antifungal and antioxidant activities. Inorg Chem Commun. 2022;143:109817. https://doi.org/10.1016/j.inoche.2022.109817.
22. Velmurugan G, Chohan JS, Paramasivam P, Maranan R. Green synthesis of silver nanoparticles from southern *Eucalyptus globulus*: potent antioxidants and photocatalysts for rhodamine B dye degradation. Desalin Water Treat. 2024;320: 100687.
23. Okumus E. Green synthesis of silver nanoparticles using *Hebeloma excedens* mushroom extract as a new source: anti-lipid peroxidation, bioaccessibility and antidiabetic properties. J Food Meas Charact. 2024;18:5157–69. https://doi.org/10.1007/s11694-024-02635-2.
24. Perera KMKG, Kuruppu KASS, Chamara AMR, Thiripuranathar G. Characterization of spherical Ag nanoparticles synthesized from the agricultural wastes of *Garcinia mangostana* and *Nephelium lappaceum* and their applications as a photo catalyzer and fluorescence quencher. SN Appl Sci. 2020;2:1974. https://doi.org/10.1007/s42452-020-03640-y.
25. Asif M, Yasmin R, Asif R, Ambreen A, Mustafa M, Umbreen S. Green synthesis of silver nanoparticles (AgNPs), structural characterization, and their antibacterial potential. Dose Response. 2022;20:15593258221088708. https://doi.org/10.1177/15593258221088709.
26. Singh P, Mijakovic I. Strong antimicrobial activity of silver nanoparticles obtained by the green synthesis in Viridibacillus sp. extracts. Front Microbiol. 2022;13:820048. https://doi.org/10.3389/fmicb.2022.820048.
27. Soliman MKY, Hashem AH, Al-Askar AA, AbdElgayed G, Salem SS. Green synthesis of silver nanoparticles from *Bauhinia variegata* and their biological applications. Green Process Synth. 2024;13:64. https://doi.org/10.1515/gps-2024-0099.
28. Chandraker SK, Lal M, Khanam F, Dhruve P, Singh RP, Shukla R. Therapeutic potential of biogenic and optimized silver nanoparticles using *Rubia cordifolia* L. leaf extract. Sci Rep. 2022;12:8831. https://doi.org/10.1038/s41598-022-12878-y.
29. Saruchi V, Kumar V, Bhatt D, Pandey S, Ghfar AA. Synthesis and characterization of silver nanoparticle embedded cellulose–gelatin based hybrid hydrogel and its utilization in dye degradation. RSC Adv. 2023;13:8409–19. https://doi.org/10.1039/D2RA03885D.
30. Dybkova S, Goncharuk O, Rieznichenko L, Terpiłowski K, Borysenko L, Gruzina T, Dybkova K, Szewczuk-Karpisz K. Aqueous dispersions of 'green' silver nanoparticles for eco-applications: synthesis, structure and biosafety. J Mol Liq. 2024;415:126319. https://doi.org/10.1016/j.molliq.2024.126319.
31. Manzoor SI, Jabeen F, Patel R, Alam Rizvi MM, Imtiyaz K, Malik MA, Dar TA. Green synthesis of biocompatible silver nanoparticles using *Trillium govanianum* rhizome extract: comprehensive biological evaluation and in silico analysis. Mater Adv. 2025;6:682–702. https://doi.org/10.1039/D4MA00959B.
32. Budhathoki S, Chaudhary N, Guragain B, Baral D, Adhikari J, Chaudhary NK. Green synthesis of silver nanoparticles from *Brassaiopsis hainla* extract for the evaluation of antibacterial and anticorrosion properties. Heliyon. 2024;10:e35642. https://doi.org/10.1016/j.heliyon.2024.e35642.
33. Korkmaz N, Ceylan Y, İmamoğlu R, Kısa D, Şen F, Karadağ A. Eco-friendly biogenic silver nanoparticles: synthesis, characterization and biological applications. Int J Environ Sci Technol. 2025;22:3707–16. https://doi.org/10.1007/s13762-024-05860-w.
34. Mehta BK, Chhajlani M, Shrivastava BD. Green synthesis of silver nanoparticles and their characterization by XRD. J Phys Conf Ser. 2017;7:12050.
35. Manik UP, Nande A, Raut S, Dhoble SJ. Green synthesis of silver nanoparticles using plant leaf extraction of *Artocarpus heterophylus* and *Azadirachta indica*. Results Mater. 2020;6:100086. https://doi.org/10.1016/j.rinma.2020.100086.
36. Asefian S, Ghavam M. Green and environmentally friendly synthesis of silver nanoparticles with antibacterial properties from some medicinal plants. BMC Biotechnol. 2024;24:5. https://doi.org/10.1186/s12896-023-00828-z.
37. Alex AM, Subburaman S, Chauhan S, Ahuja V, Abdi G, Tarighat MA. Green synthesis of silver nanoparticle prepared with Ocimum species and assessment of anticancer potential. Sci Rep. 2024;14:11707. https://doi.org/10.1038/s41598-024-61946-y.
38. Wattimena SC, Silooy DR, Patty PJ. Characterization of green silver nanoparticles of *Graptophyllum pictum* leaf extract: from the localized surface plasmon resonance to the antimicrobial activity. J Phys Conf Ser. 2021;8:12065.

39. Sharma A, Sagar A, Rana J, Rani R. Green synthesis of silver nanoparticles and its antibacterial activity using fungus *Talaromyces purpureogenus* isolated from *Taxus baccata* Linn. Micro Nano Syst Lett. 2022;10:2. https://doi.org/10.1186/s40486-022-00144-9.
40. Sahu SK, Mansoori A, Jana SK, Kumar A, Ghorai TK. Biosynthesis of silver nanoparticles using green tea aqueous leaf extract and their biological and chemotherapeutic activity. J Mol Struct. 2025;1320:139690. https://doi.org/10.1016/j.molstruc.2024.139690.
41. Hashemi Z, Mizwari ZM, Mohammadi-Aghdam S, Mortazavi-Derazkola S, Ali Ebrahimzadeh M. Sustainable green synthesis of silver nanoparticles using *Sambucus ebulus* phenolic extract (AgNPs@SEE): optimization and assessment of photocatalytic degradation of methyl orange and their in vitro antibacterial and anticancer activity. Arab J Chem. 2022;15:103525. https://doi.org/10.1016/j.arabjc.2021.103525.
42. Ramya JR, Ali S, Vijayalakshmi R, Gajendiran J, Gnanam S, Ramachandran K. Antimicrobial efficiency against fish pathogens on the green synthesized silver nanoparticles. Microb Pathog. 2024;193:106725. https://doi.org/10.1016/j.micpath.2024.106725.
43. Hillyer MB, Jordan JH, Nam S, Easson MW, Condon BD. Silver nanoparticle-intercalated cotton fiber for catalytic degradation of aqueous organic dyes for water pollution mitigation. Nanomaterials. 2022. https://doi.org/10.3390/nano12101621.
44. Cyril N, George JB, Joseph L, Sylas VP. Catalytic degradation of methyl orange and selective sensing of mercury ion in aqueous solutions using green synthesized silver nanoparticles from the seeds of *Derris trifoliata*. J Clust Sci. 2019;30:459–68. https://doi.org/10.1007/s10876-019-01508-9.
45. Marques NRS, Lima MTA, Pereira GAL, Pereira G. Catalytic degradation of azo dyes by silver nanoparticles. Eng Proc. 2023. https://doi.org/10.3390/ASEC2022-13952.
46. Rajasekar R, Thanasamy R, Samuel M, Edison TNJI, Raman N. Ecofriendly synthesis of silver nanoparticles using *Heterotheca subaxillaris* flower and its catalytic performance on reduction of methyl orange. Biochem Eng J. 2022;187:108447. https://doi.org/10.1016/j.bej.2022.108447.
47. Sherin L, Sohail A, Amjad US, Mustafa M, Jabeen R, Ul-Hamid A. Facile green synthesis of silver nanoparticles using *Terminalia bellerica* kernel extract for catalytic reduction of anthropogenic water pollutants. Colloid Interface Sci Commun. 2020;37:100276. https://doi.org/10.1016/j.colcom.2020.100276.
48. Alamier WM, Oteef MDY, Bakry AM, Hasan N, Ismail KS, Awad FS. Green synthesis of silver nanoparticles using acacia ehrenbergiana plant cortex extract for efficient removal of rhodamine B cationic dye from wastewater and the evaluation of antimicrobial activity. ACS Omega. 2023;8:18901–14. https://doi.org/10.1021/acsomega.3c01292.

Publisher's Note Springer Nature remains neutral with regard to jurisdictional claims in published maps and institutional affiliations.